

Article

# Investigation of the Leaching Kinetics of Zinc from Smithsonite in Ammonium Citrate Solution

Huiqin Chen, Dandan Wu \* and Ziang Wang

State Key Laboratory of Complex Nonferrous Metal Resources Clean Utilization, Kunming University of Science and Technology, Kunming 650093, China; cpp1317@163.com (H.C.); boojum1999@163.com (Z.W.)

\* Correspondence: wdd1006530@sina.com

**Abstract:** In this study, the response surface method is used to develop a model for analyzing and optimizing zinc leaching experiments. An investigation into the leaching kinetics of smithsonite in ammonium citrate solution is also conducted. A model of kinetics is studied in order to represent these effects. The experimental data show that an increase in the solution temperature, concentration, and stirring speed has a positive impact on the leaching rate, while an increase in the particle size has a negative impact on it. The optimal experimental conditions consist of a leaching temperature of 70 °C, ammonium citrate concentration of 5 mol/L, particle size of 38 μm, and rotational speed of 1000 rpm. Under these optimal conditions, the leaching rate of zinc from smithsonite is 83.51%. It is speculated that the kinetic model will change when the temperature is higher than 60 °C. When the temperature is lower than 60 °C, the leaching process is under the control of the shrinking core model of the surface chemical reactions. The calculated activation energy of the leaching reaction is equal to 42 kJ/mol. The model of the leaching process can be described by the following equation:  $1 - (1 - x)^{1/3} = [k_0 \cdot (C)^{0.6181} \cdot (r_0)^{-0.5868} \cdot (SS)^{0.6901} \exp(-42/RT)] t$ . This demonstrates that an ammonium citrate solution can be used in the leaching process of zinc in smithsonite as an effective and clean leaching agent.

**Keywords:** dissolution; smithsonite; ammonium citrate; kinetics; response analysis



**Citation:** Chen, H.; Wu, D.; Wang, Z. Investigation of the Leaching Kinetics of Zinc from Smithsonite in Ammonium Citrate Solution. *Metals* **2024**, *14*, 519. <https://doi.org/10.3390/met14050519>

Academic Editors: Ilhwan Park and Alexandre Chagnes

Received: 20 February 2024

Revised: 22 April 2024

Accepted: 25 April 2024

Published: 29 April 2024



**Copyright:** © 2024 by the authors. Licensee MDPI, Basel, Switzerland. This article is an open access article distributed under the terms and conditions of the Creative Commons Attribution (CC BY) license (<https://creativecommons.org/licenses/by/4.0/>).

## 1. Introduction

Zinc is a non-ferrous metal that plays an indispensable role in the construction industry, with its consumption trailing only that of iron, aluminum, and copper. Zinc chemicals and rolled zinc are widely used in galvanization industries [1,2]. Zinc can be extracted from some industrial waste residues or recycled materials, and zinc recovered from waste accounts for almost 40% of the recovered zinc. For example, in the process of steel production, zinc-containing dust will be produced. Zinc in these wastes can be recovered and refined through specific processes. Similarly, some waste electronic products and batteries also contain zinc, and zinc metal can also be extracted by recycling and treating these materials [3,4]. At present, zinc mainly comes from the mining and refining of mineral resources [5,6].

Due to the ease of separating sulfides from gangue minerals with conventional flotation methods, zinc sulfide ores are currently the main material for the production of zinc [7]. However, with the increasing demand for zinc and shortage of high-grade zinc sulfide resources with exploitable value worldwide, meeting the production demand using only zinc sulfide resources became difficult [8,9]. Thus, the industrial production of zinc using zinc oxide ore has gradually become an inevitable way for the development of non-ferrous metallurgy [10,11]. Compared with zinc sulfide ore, zinc oxide ore has a more complex composition. It mainly includes *hemimorphite* [ $Zn_4Si_2O_7(OH)_2 \cdot H_2O$ ], *wurtzite* ( $Zn_2SiO_4$ ), and *smithsonite* ( $ZnCO_3$ ) [12–14]. Among them, smithsonite is the most abundant non-zinc sulfide mineral, and its extraction has been widely studied [15].

The technology used in the treatment of zinc oxide ore mainly includes pyrometallurgy and hydrometallurgy [16]. In past decades, pyrometallurgical research has been carried out on the treatment of low-grade zinc oxide ore. However, the traditional pyrometallurgical process consumes a lot of energy and produces a lot of off-gases and waste residue, which causes serious environmental pollution [17–19]. Therefore, under the conditions of increasingly strained energy and strict environmental protection requirements, pyrometallurgy is gradually being replaced by hydrometallurgy. The hydrometallurgical process is to use an acid or alkali solution to react with zinc oxide ore, so as to dissolve zinc, and then produce metal zinc or zinc compound through subsequent treatment. It has the advantages of strong selectivity, low energy consumption, simple operation, high comprehensive recovery rate of resources, and little environmental pollution [20–22].

The leaching process is the first stage of hydrometallurgy. It significantly affects the economic enrichment of metal minerals [23]. According to different leaching agents, the hydrometallurgical process of zinc oxide ore is mainly divided into three methods: acid leaching, ammonia leaching, and alkali leaching [24–26]. Alkali leaching uses NaOH leaching. This process is similar to acid leaching, while it avoids some drawbacks faced by the latter [27–29]. The alkaline leaching equipment results in slow corrosion, simple solid–liquid separation, easy purification of leaching solution, and more environmental protection compared with ammonia leaching. However, when treating low-grade zinc oxide ore, the alkali level in the leaching residue is high and the viscosity of the leaching solution is high, which leads to a low zinc recovery rate. Therefore, it has not been widely used in the industry. The ammonia leaching adopts the ammonia, or ammonia plus ammonium salt, as its leaching agent. This method is able to perform selective leaching of zinc while avoiding many common problems, such as silica gel. However, ammonia has high volatility, which results in significant losses in the operation process. This not only increases the production cost, but also worsens the operating environment [8,30–32].

Compared with ammonia leaching and alkali leaching, acid leaching has obvious advantages in treating minerals. For example, it has higher leaching efficiency and more economical operating conditions. Acid leaching can be performed with organic or inorganic acids. Sulfuric acid is the most commonly used inorganic acid leaching agent for zinc oxide ores [33–35]. However, in general, zinc oxide ores contain high silicate, which increases the consumption of sulfuric acid, generates silica gel, which is difficult to treat, and affects the separation [36,37]. Organic acids usually have lower corrosivity and less pollution to the environment compared with inorganic acids. Feng et al. [38] studied the leaching kinetics of smithsonite in a methanesulfonic acid (MSA) solution. Their results showed that the leaching rate of zinc is positively correlated with an increase in the MSA concentration, reaction temperature, and stirring speed, while it is negatively correlated with an increase in the particle size. The kinetics of hemimorphite dissolution in the presence of trichloroacetic acid (TCAA) were investigated by Zhang et al. [39]. The results show that the leaching rate of zinc is proportional to the increase in reaction temperature, TCAA concentration, and stirring speed, as well as a decrease in particle size. Their results also showed that zinc rapidly dissolves in TCAA during the whole leaching process. Irannajad et al. [40] studied the leaching of low-grade zinc oxide tailings with organic acid, using citric acid as a leaching agent. Their results showed that under the optimum conditions, the recovery rate of zinc is 82%. Shokrullah et al. [41] investigated 17 various leaching agents, comprising inorganic and organic acids, alkaline solutions, and chelating agents to extract zinc from flotation tailings. Their findings revealed that, apart from sulfuric acid, organic acids like citric acid, malic acid, and sulfosalicylic acid demonstrate favorable leaching efficiencies on zinc oxide ore.

The purpose of this study is to provide an alternative method for leaching zinc from smithsonite and to explore the influence of the experimental parameters. Ammonium citrate (AC) is a crucial organic acid salt which has very high solubility. Compared with the traditional leaching agent, ammonium citrate has lower toxicity and causes less harm to the environment. In addition, the waste liquid produced in the leaching process of ammonium

citrate can be easily treated. Li et al. [42] studied the impact of ammonium citrate on the alkaline leaching of hemimorphite. They discovered that the reactants needed to dissolve hemimorphite are  $\text{NH}_4^+$  ions and  $\text{NH}_3$  molecules. The concentration of  $\text{NH}_4^+$  ions in the leachate increases with the increase in AC concentration, which is helpful to promote the chemical process and thus facilitates the recovery of zinc.

Few studies exist on the impact of ammonium citrate as a leaching agent on smithsonite leaching. Thus, in order to improve the acid leaching of zinc oxide ore, this paper considers ammonium citrate (AC) as a novel leaching agent to study the leaching kinetics of smithsonite. This aims at improving the theory of reaction between organic acids and zinc oxide ore. The impacts of many factors, such as the ammonium citrate concentration, temperature, stirring speed, and particle size, on the zinc leaching were also studied, and the best leaching conditions were deduced. In addition, the leaching reaction model of zinc in ammonium citrate was developed by establishing an accurate equation.

## 2. Materials and Methods

### 2.1. Materials

The samples of smithsonite used in the experiment were produced in Lanping lead-zinc mine, Yunnan Province, China. The massive smithsonite samples were first crushed by hand, ground with a three-head mill, and finally screened using a standard test screen to obtain powder samples of different particle sizes in order to meet the sample size requirements for the dissolution test. A Rigaku D/max 2550VB + 18 kW powder diffractometer (Rigaku, Tokyo, Japan), which contains a Cu target  $\text{K}\alpha$  X-ray source at 40 kV and 40 mA, was then used to conduct the mineralogical analysis of the mineral samples. The results of the X-ray analysis are shown in Figure 1, where the smithsonite and quartz are considered as the constituents of the samples. Table 1 shows the chemical multi-element analysis data of smithsonite. It can be seen that the zinc content of mineral smithsonite is 49.46% by chemical titration, while its theoretical content is 52.15%, which indicates that the sample has high purity.

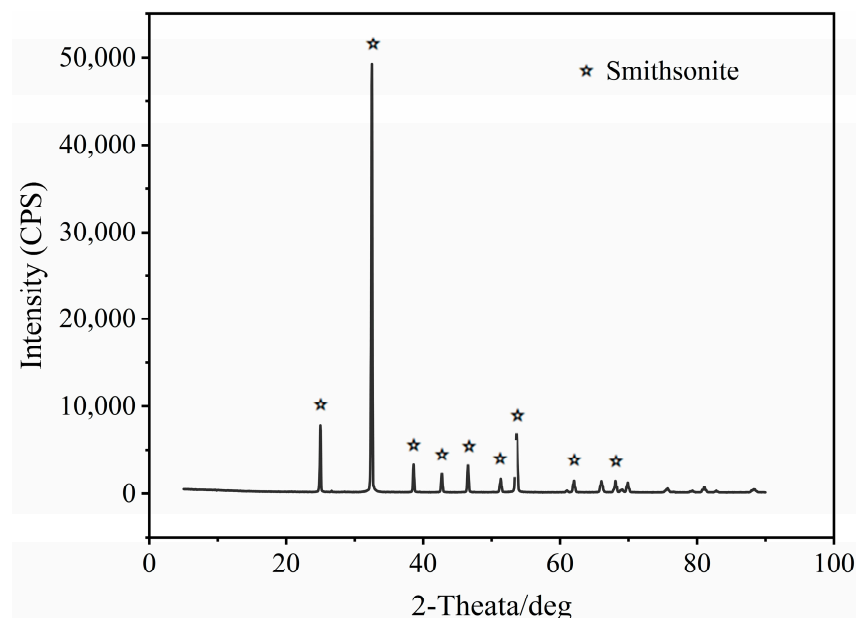


**Figure 1.** X-ray diffraction pattern of original smithsonite sample.

**Table 1.** Chemical composition of pure smithsonite samples.

Elements	Zn	Fe	CaO	$\text{Al}_2\text{O}_3$	Pb	Cd	$\text{SiO}_2$
Content %	49.46	0.4	0.59	0.50	0.67	0.46	1.74

## 2.2. Optimal Experimental Design

RSM can accurately evaluate the relationship between each component and the response value by establishing a mathematical model, which includes the first-order, square, and first-order interactions between any two elements. RSM is a systematic process modeling and optimization method, aiming at finding the ideal conditions of multi-factor systems rapidly and effectively [43]. The Box–Behnken design (BBD) was used for this study's experimental design. A BBD evaluation approach of the experimental design was used to gauge the nonlinear interaction between variables. The composite number of elements in the BBD test group was relatively lower and more cost effective compared to the central composite design. Moreover, it requires fewer consecutive trials [44–47].

The multiple linear regression model was employed to conduct modeling and fitting analysis, while the Design-Expert13 program was employed for the optimization experiment. The graphical and numerical optimization features of the software were employed to determine the ideal leaching conditions. The multiple linear regression model is obtained by

$$Y = a_0 + \sum_{i=1}^k a_i k_i + \sum_{i=1}^k a_{ii} x_i^2 + \sum_{i=1}^k \sum_{j=1}^k a_{ij} x_i x_j \quad (1)$$

where  $k$  represents the quantity of experimental factors,  $y$  denotes the response value,  $a_0$  signifies the model constant,  $x_i$  and  $x_j$  are the experimental parameters,  $a_i$  stands for the linear coefficient,  $a_{ij}$  represents the interaction coefficient, and  $a_{ii}$  indicates the quadratic coefficient.

The selected level and range, obtained by considering the temperature, ammonium citrate concentration, particle size, and stirring speed as variable factors, are shown in Table 2.

**Table 2.** Levels and codes of factors for BBD.

Factors	Symbol	Coding Level		
		−1	0	1
Temperature (°C)	A	30	50	70
Ammonium citrate concentration (mol/L)	B	1	3	5
Particle size (μm)	C	38	176.5	315
Stirring speed (rpm)	D	200	600	1000

## 2.3. Experimental Procedure

The leaching process took place in a 1000 mL three-necked flask batch reactor, which was heated by a thermostat to maintain a constant temperature for all the contents during the process. Other devices equipped in the reactor included a mechanical stirrer controlled by a digital stirrer, a thermometer that controls the reaction temperature, and a condenser that controls the evaporation loss. In this experiment, 5 g of smithsonite powder sample were mixed with 1000 mL of freshly prepared ammonium citrate solutions of specific concentrations. A total of 5 mL of the samples were extracted from the solution after mixing and then used for analysis. The zinc leaching rate was determined by measuring the zinc content in the solution using inductively coupled plasma atomic emission spectrometry (ICP) (Nexion 2000 ICP-MS, Acton, MA, USA). The surface morphology and semi-quantitative analysis of elements before and after mineral leaching were characterized by scanning electron microscopy (SEM-EDS) (Tescan Mira Lms, Brno, Czech Republic).

In the experiments, a control variable was used to study the impacts of the reaction temperature, concentration of ammonium citrate, particle size, and stirring speed on the smithsonite leaching. Four groups of experiments, having the same experimental conditions, were conducted. They are highlighted by an asterisk in Table 3. In this study, all the experiments were repeated at least 3 times, and the average of the obtained results was considered.

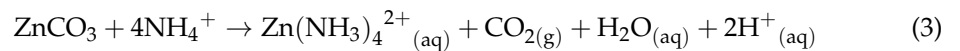
**Table 3.** Leaching parameters and ranges used in leaching experiments.

Parameter	Value
Concentration (mol/L)	1, 2, 3, 4 *, 5
Temperature (°C)	30, 40, 50, 60 *, 70
Stirring speed (rev/min)	200, 400, 600, 800 *, 1000
Particle size (µm)	38, 60, 122.5, 200 *, 315

\* These parameters were kept constant.

### 3. Results and Discussion

By forming a stable  $\text{Zn}(\text{NH}_3)_4^{2+}$  complex, smithsonite ( $\text{ZnCO}_3$ ) dissolves in an ammonium citrate ( $\text{C}_6\text{H}_7\text{O}_7(\text{NH}_4)_3$ ) solution. The reactions between the smithsonite and ammonium citrate solution can be expressed as:



Therefore, the overall leaching reaction is obtained by:



#### 3.1. Impact of Temperature on Smithsonite Leaching

In order to study the impact of the reaction temperature on smithsonite leaching, many tests, lasting for 30 min each, were conducted. The experiments were conducted at a temperature in the range of 30–70 °C, with an ammonium citrate concentration of 4 mol/L, a solid/liquid ratio of 1/200 g/mL, a stirring speed of 800 rpm, and particle sizes of 60 µm. The obtained results are shown in Figure 2.

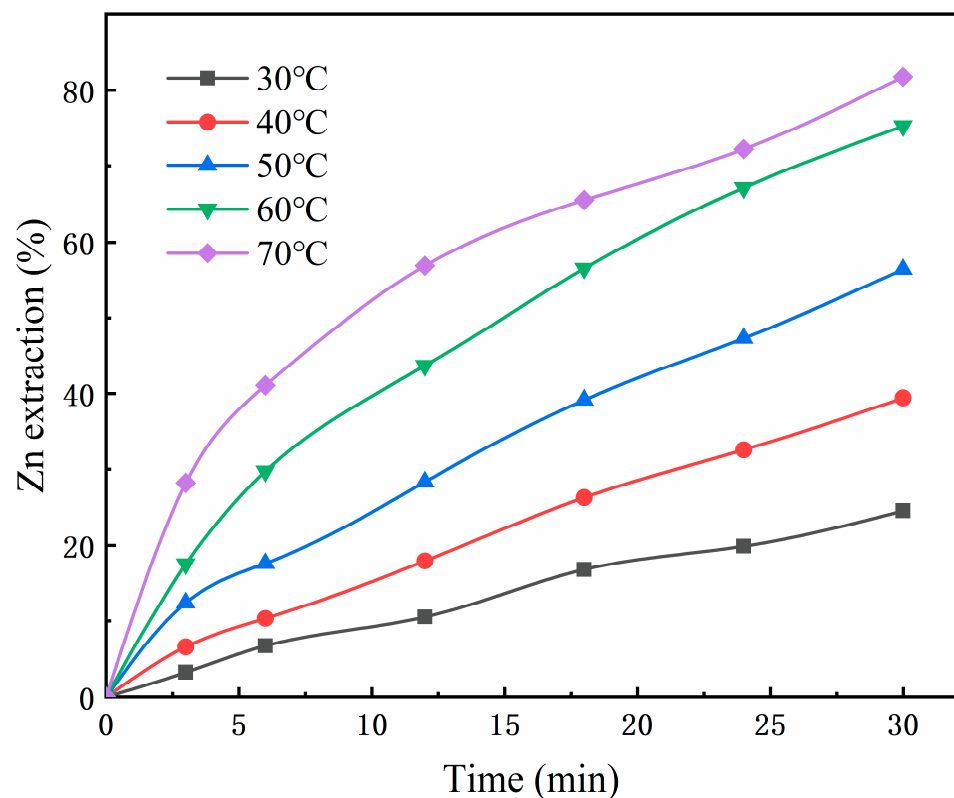


**Figure 2.** Effect of reaction temperature on dissolution of smithsonite.

The rate of zinc extraction from smithsonite significantly increases with an increase in temperature under the previously described experimental conditions. In particular, when the temperature increases from 30 °C to 70 °C, the level of zinc extraction increases from 24.57% to 81.78%.

### 3.2. Impact of the Ammonium Citrate Concentration on Smithsonite Leaching

Five distinct ammonium citrate concentrations, ranging between 1 mol/L to 5 mol/L, were adopted in the experiments. The other process parameters remained constant. More precisely, they consist of a temperature of 60 °C, a stirring speed of 800 rpm, a solid/liquid ratio of 1/200 g/mL, and a particle size of 60 µm. Figure 3 shows the results of leaching rates obtained under different concentrations of ammonium citrate solution.

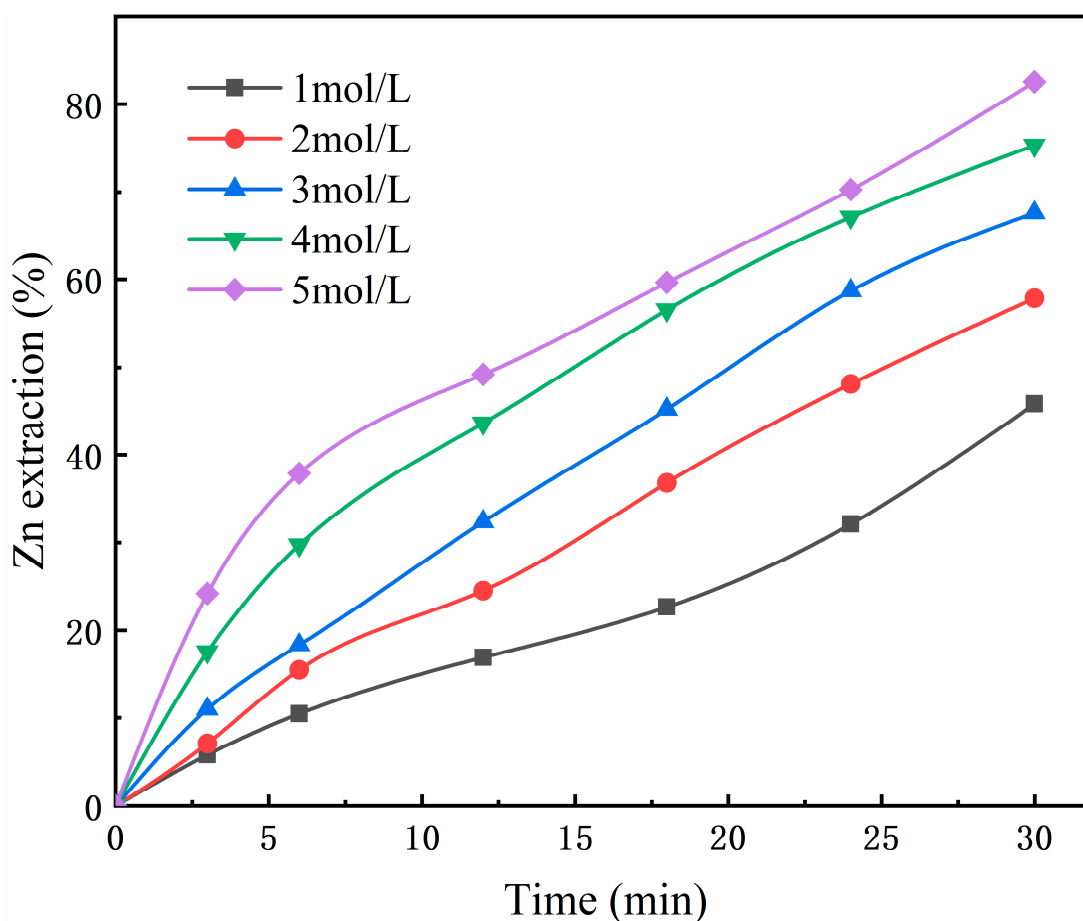


**Figure 3.** Effect of ammonium citrate concentration on dissolution of smithsonite.

It is evident that as the concentration of ammonium citrate rises, so does the rate at which zinc leaches. More precisely, when the concentration of ammonium citrate increases from 1 mol/L to 5 mol/L, the level of zinc extraction increases from 45.86% to 82.51%. In addition, the concentration of ammonium citrate is the most important factor affecting the dissolution of smithsonite.

### 3.3. Impact of the Particle Size on Smithsonite Leaching

Experiments with five particle sizes (38, 60, 122.5, 200, and 315 µm) were conducted to study the impact of the particle size and other factors on the leaching of smithsonite. The temperature, ammonium citrate concentration, and stirring speed were fixed at 60 °C, 4 mol/L, and 800 rpm, respectively. The results obtained are shown in Figure 4. It can be seen that, when the particle size decreases, the rate of zinc leaching increases.

In addition, increasing the particle size has a negative impact on the leaching rate of zinc. More precisely, when the particle size increases from 38  $\mu\text{m}$  to 315  $\mu\text{m}$ , the leaching rate decreases from 82.19% to 31.82%. The leaching rate can reach 82.19% for a particle size of 38  $\mu\text{m}$  and a reaction time of 30 min. This is due to the fact that when the particle size increases, the ratio of surface area to volume of mineral particles will decrease. This means that the contact surface area between the leaching agent and zinc species on the mineral surface is reduced, which leads to a decrease in the reaction rate and further affects the leaching rate of zinc.

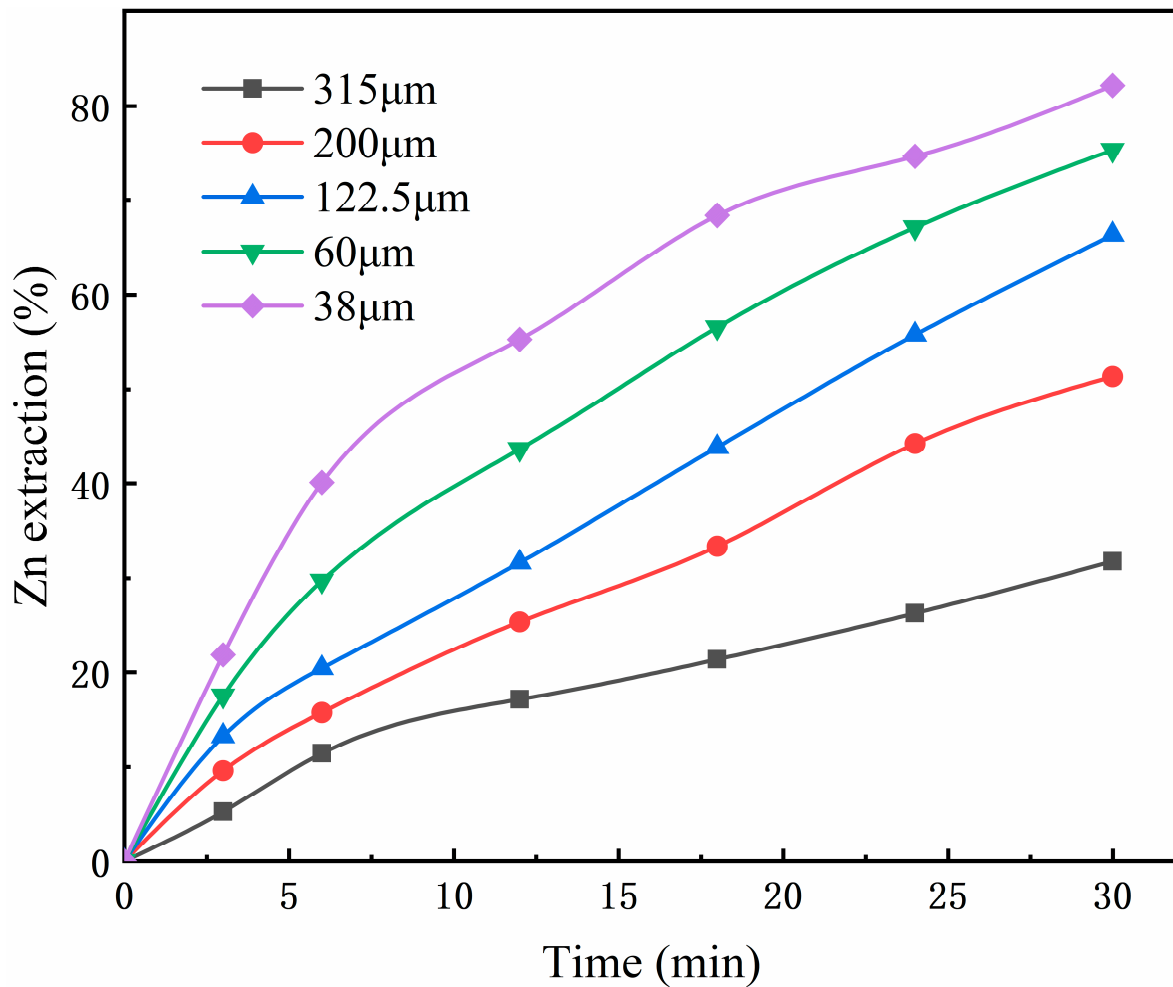


**Figure 4.** Effect of particle size on dissolution of smithsonite.

#### 3.4. Impact of Stirring Speed on Smithsonite Leaching

Experiments were conducted to study the impact of stirring speed on the leaching of zinc. The stirring speed was varied (200, 400, 600, 800, 1000 rpm) while the other factors affecting the smithsonite leaching were fixed (temperature of 60  $^{\circ}\text{C}$ , ammonium citrate concentration of 4 mol/L, and particle size of 60  $\mu\text{m}$ ).

The results obtained are shown in Figure 5. It can be seen that, when the stirring speed increases from 200 rpm to 1000 rpm, the leaching rate of zinc in the solution is significantly improved from 39.45% to 80.86%.

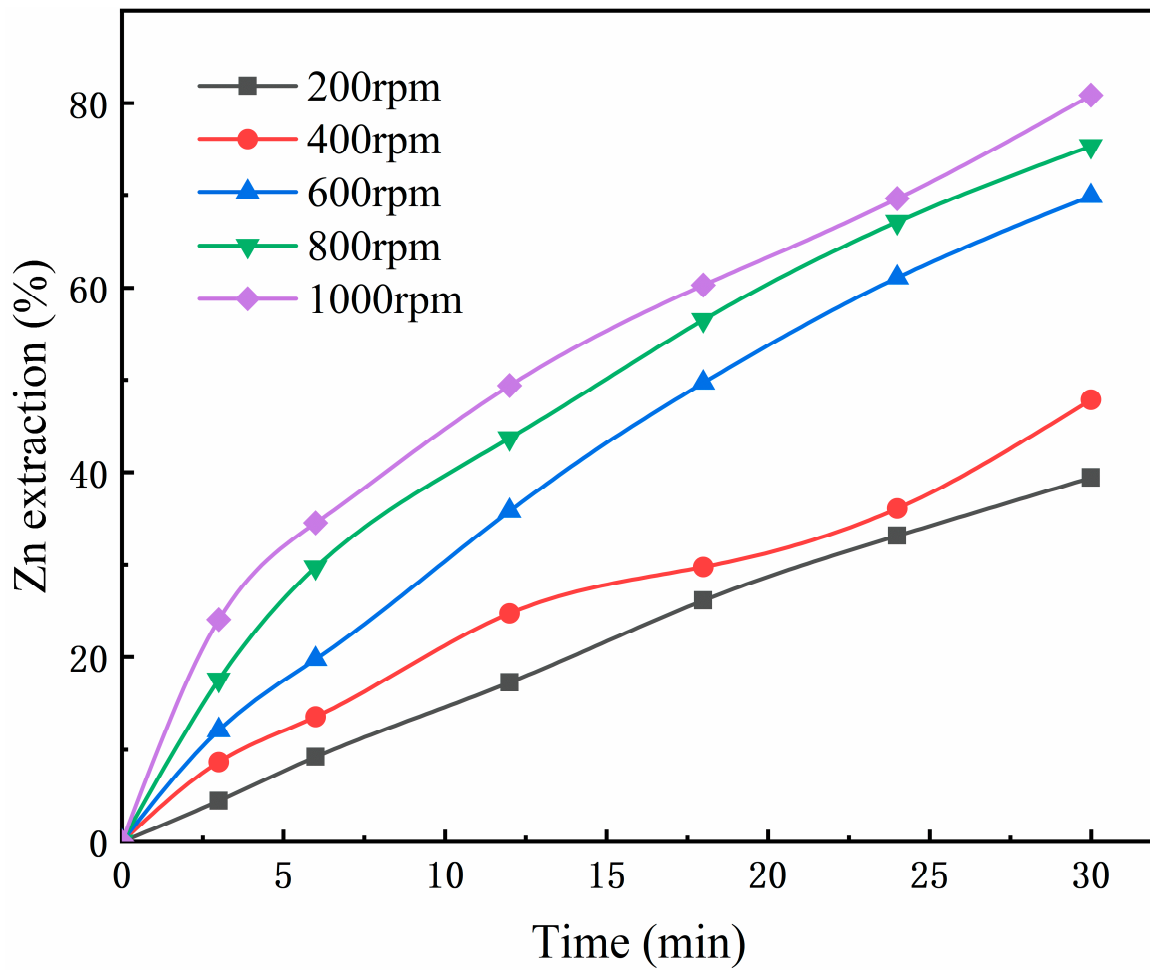


Figure 5. Effect of stirring speed on dissolution of smithsonite.

3.5. Statistical Analysis and Model Fitting

3.5.1. Data Analysis

Table 4 displays the results of the analysis of variance (ANOVA) for the zinc leaching response surface model in the smithsonite.

Table 4. ANOVA for response surface quadratic model.

	Sum of Squares	df	Mean Square	F-Value	p-Value	
Model	12,515.20	10	1251.52	58.64	<0.0001	significant
A-Temperature	2928.43	1	2928.43	137.21	<0.0001	
B-Ammonium citrate concentration	1433.21	1	1433.21	67.15	<0.0001	
C-Particle size	1652.12	1	1652.12	77.41	0.0003	
D-stirring speed	220.18	1	220.18	10.32	0.0048	
AB	23.30	1	23.30	1.09	0.3100	
AC	337.83	1	337.83	15.83	0.0009	
AD	59.79	1	59.79	2.80	0.0661	
BD	45.24	1	45.24	2.12	0.0008	
A <sup>2</sup>	237.91	1	237.91	11.15	0.0002	
B <sup>2</sup>	127.84	1	127.84	5.99	0.0565	
Residual	384.14	18	21.34			
Lack of Fit	366.54	17	21.56	1.22	0.6217	not significant

The F-value is a statistically sound measure of the existing variance in ANOVA. The F-value of the model, which is equal to 58.64, indicates that it is significant based on ANOVA. There is barely a 0.1% chance of attaining such a high F-value due to the noise. If the *p*-value for the quadratic model is less than 0.0001, it is considered significant. In fact, a *p*-value less than 0.05 denotes significance. In this scenario, the model terms A, B, C, D, AC, BD, and A<sup>2</sup> are significant. The influence of the significant model term can be increased by reducing the equation to the most significant variable with just 95% confidence. The following regression equation can then be obtained:

$$E(Zn) = 44.76 + 15.96A + 12.54B - 11.21C + 4.31D - 7.77AC + 3.645BD - 6.69A^2 \tag{5}$$

To enhance the evaluation of the data-fitting capability of the quadratic model, a few important diagnostic maps were created. The majority of the experimental data points were situated along the diagonal axis as illustrated in Figure 6a, which indicates that there was little departure, and the data were typically reliable. The error components have a normal distribution, and they are independent due to the fact that the residuals' normal distribution essentially follows a straight line. The random distribution of the points close to zero on the outlier *t*-axis and between  $-3.7412$  and  $3.7412$  in Figure 6b,c confirms that the quadratic model successfully established the link between the key experimental variables and the leaching rate.

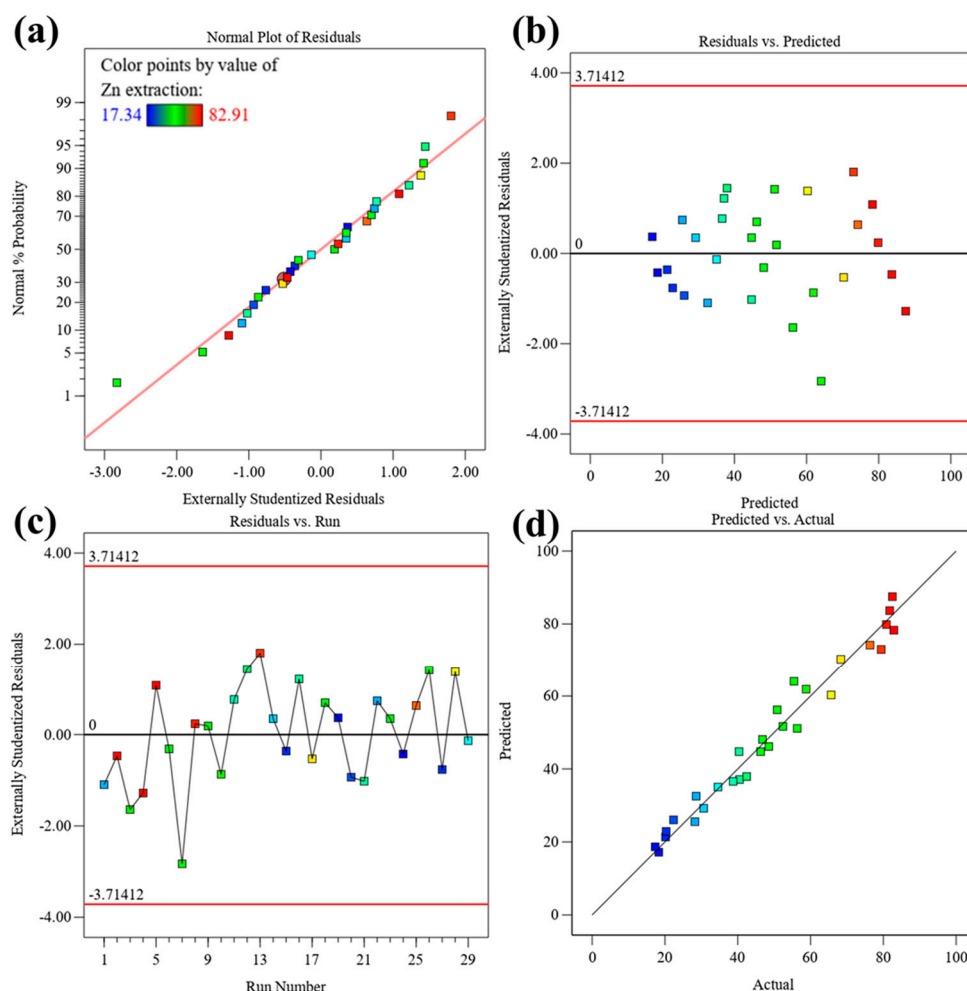


**Figure 6.** (a) A plot of normal probability vs. the internally studentized residuals, (b) internally studentized residuals vs. the predicted responses, (c) internally studentized residuals vs. run number, and (d) predicted responses vs. the actual values.

Figure 6d shows a comparison chart between the expected and actual values. It can be seen that the slope is near 1, the points are mostly dispersed in a straight line, and the actual and anticipated results are consistent. The perturbation for zinc extraction efficiency (A: temperature; B: ammonium citrate concentration; C: particle size; D: stirring speed) is then drawn, as shown in Figure 6. It can be observed that the accuracy of the quadratic model can forecast the true value and the dependability of the experimental findings. The zinc leaching rate in the smithsonite is significantly affected by the temperature, ammonium citrate content, particle size, and stirring speed, as shown in the aforementioned difference analysis.

### 3.5.2. Internal Relationships between Factors

The coefficients A, B, C, and D are 15.96, 12.54,  $-11.21$ , and 4.31 (Equation (5)), respectively. These coefficients show the extent of the impact of a factor on the response value [48,49]. It can be clearly seen from the aforementioned equations that, except for the particle size, all the other parameters have a positive impact on the leaching rate of zinc. In addition, the order of predominance influencing the leaching rate is given by the following: Rotation speed (D) > Temperature (A) > Ammonium citrate concentration (B) > Particle size (C).

The two-dimensional contour map and three-dimensional response surface map derived from the secondary model reflect how these variables interact with the response values. Figure 7a,b show the interaction of the temperature and ammonium citrate concentration on the zinc leaching rate. The three-dimensional response surface plots show that, when the temperature and the ammonium citrate concentration increase, the surface gradually steepens. Under the condition of low concentration (1 mol/L) of ammonium citrate, the leaching rate still increases above 70 °C. At a certain temperature, when the ammonium citrate concentration increases, the leaching rate gradually increases and then stabilizes. This indicates that, when the leaching rate reaches its maximum value, the amount of ammonium citrate solution used in the experiment can be decreased. In addition, the two-dimensional contour plots demonstrate that the temperature has a greater impact on the leaching rate compared with the ammonium citrate concentration. Figure 7c,d show the impacts of the temperature and particle size ratio on the efficiency of the zinc leaching process, respectively. It can be seen that the surface gradually steepens with an increase in the temperature and the particle size. In addition, when the particle size increases, the leaching rate decreases and the surface slopes become lower. Also, the temperature has a greater impact on the leaching rate compared with the particle size. The interaction of temperature and rotational speed affects the leaching efficiency of zinc, as shown in Figure 7e,f. Moreover, the leaching surface steepens with an increase in the temperature and the stirring speed. Furthermore, the influence of temperature on the leaching rate is of greater importance compared to the stirring velocity. The interaction of ammonium citrate concentration and rotational speed affects the leaching efficiency of zinc, as shown in Figure 7g,h. It can also be seen that the leaching surface steepens with an increase in the ammonium citrate concentration and the stirring speed. Moreover, the ammonium citrate concentration has a greater impact on the leaching rate compared with the stirring speed. The influence on the leaching rate increases with an increase in the contour tilt. In line with the order of the F-value, the interaction sequence is as follows: AC > AD > BD > AB.

Each factor interaction term has extreme value points, as shown in Figure 7. The Design Expert 13 software was used to predict the zinc leaching rate from smithsonite at temperature of 68.359 °C, ammonium citrate concentration of 4.395 mol/L, particle size of 38.336  $\mu\text{m}$ , and rotational speed of 952.443 rpm. A result of 83.6685 was obtained. The optimal experimental conditions were then modified to make the experiment easier to perform. The optimized leaching temperature, ammonium citrate concentration, particle size, and rotational speed were considered equal to 70 °C, 5 mol/L, 38  $\mu\text{m}$ , and 1000 rpm, respectively. The zinc leaching rate from smithsonite under the best circumstances was equal

to 83.51%, which is consistent with the expected value of 83.668%. This provides additional validation regarding the excellent precision of the model within the response surface.

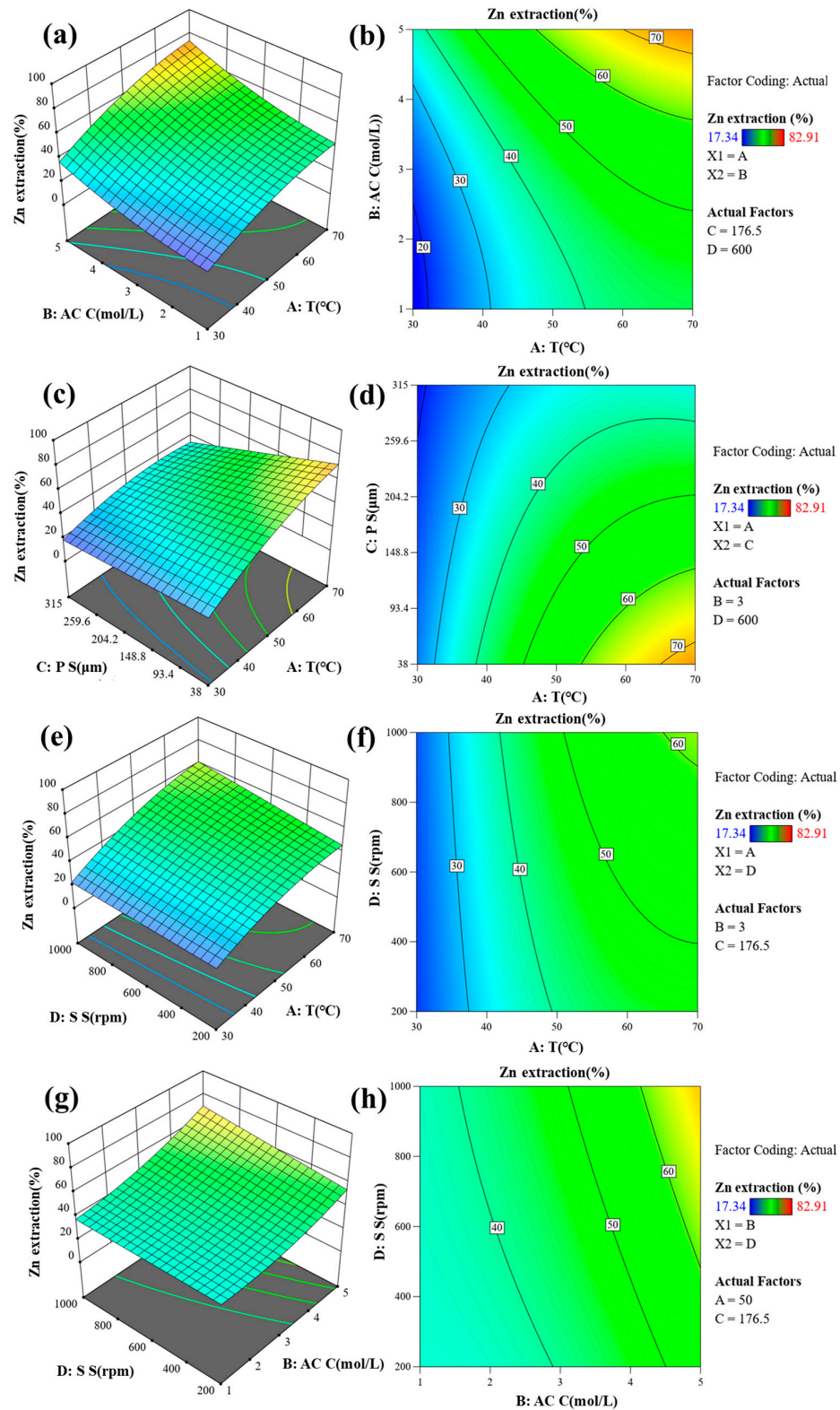


**Figure 7.** Three-dimensional response surface and contour plots (other parameters are held at the center level) showing the combined effects of T and AC C (a,b); T and PS (c,d); T and SS (e,f); AC C and PS (g,h) (T is temperature, AC C is ammonium citrate concentration, PS is particle size, SS is stirring speed).

### 3.6. Kinetics Study

A heterogeneous liquid–solid reaction took place during the leaching of smithsonite using ammonium citrate. When smithsonite interacts with the leaching agent solution, only a part of zinc is leached. The reaction between the mineral particles and leaching reagent in the solution can be expressed as [50]



where  $a$  and  $b$  are the stoichiometric coefficients and  $A(s)$  and  $B(aq)$  denote the solid that is being leached and the reactant in the solution, respectively.

In general, the shrinking-core model can be used to explain the kinetics of the leaching process. In this model, aqueous and solid products are formed on the surface of the solid particles due to the reaction of reactants on it. When conducting the reaction, the unreacted core of the solid will shrink towards the center, a layer of porous products around the unreacted nucleus will form, and the more solid and aqueous products will be produced. According to this model, the following steps are usually considered in the leaching process: (1) liquid film diffusion control, (2) diffusion control of the solid product layer, and (3) control of the surface chemical reaction.

If the leaching rate is controlled by external diffusion, the comprehensive rate equation is expressed as [51–55]:

$$x = k_1 t \quad (7)$$

If the reaction is under the control of a surface chemical reaction, the integrated rate equation can be expressed as [51–55]:

$$1 - (1 - x)^{1/3} = k_r t \quad (8)$$

If the reaction rate is controlled by the diffusion of the product layer, the integrated rate equation of this step is written as [51–55]

$$1 - (1 - x)^{2/3} - 2/3x = k_d t \quad (9)$$

where  $x$  is the conversion percentage of solid particles,  $k_1$  is the apparent rate constant diffusing through the fluid film,  $k_r$  is the apparent rate constant diffusing through the surface chemical reaction,  $k_d$  is the apparent rate constant diffusing through the product layer, and  $t$  is the reaction time.

Equations (7)–(9), based on the shrinking core model, were used to manage the experimental data, in order to determine the rate-controlling step of dissolution. The apparent rate constants and corresponding  $R^2$  values of the three kinetic models are listed in Table 5. The results obtained by Equations (8) and (9) are shown in the third and fourth columns of Table 5, respectively. In addition, the second column of Table 5 shows the results obtained by fitting Equation (7). It can be seen that the results of Equation (8) have larger regression coefficients compared with those of Equations (9) and (7). This shows that the leaching kinetics of smithsonite in this system accords with the surface chemical reaction control model. The fitting curves of  $1 - (1 - x)^{1/3}$  with time at different temperature, solution concentration, stirring speed, and particle size are shown in Figure 8. The validity of the leaching model of smithsonite in ammonium citrate solution is verified. Therefore, enhancing the leaching efficiency involves elevating the leaching agent concentration, reaction temperature, stirring speed, and decreasing the size of the initial particles.

**Table 5.** Apparent rate constants  $k_l$ ,  $k_r$ , and  $k_d$  for the kinetic models and correlation.

Parameter	Diffusion through the Liquid Film		Surface Chemical Reaction		Diffusion through the Product Layer					
	$x$	$1 - (1 - x)^{1/3}$	$1 - (1 - x)^{1/3}$	$1 - 3(1 - x)^{2/3} + 2(1 - x)$	$k_l$ (min <sup>-1</sup> )	$R^2$	$k_r$ (min <sup>-1</sup> )	$R^2$	$k_d$ (min <sup>-1</sup> )	$R^2$
Temperature [K (°C)]										
293 (30)	0.0073	0.991	0.0026	0.990	0.0005	0.896				
303 (40)	0.0128	0.997	0.0048	0.999	0.0002	0.877				
313 (50)	0.0207	0.942	0.0085	0.981	0.0015	0.936				
323 (60)	0.0284	0.897	0.0130	0.979	0.0031	0.961				
333 (70)	0.0339	0.700	0.0172	0.921	0.0049	0.987				
Concentration (mol/L)										
1	0.0143	0.981	0.0055	0.963	0.0007	0.763				
2	0.0199	0.993	0.0082	0.997	0.0014	0.881				
3	0.0241	0.982	0.0104	0.999	0.0022	0.904				
4	0.0284	0.897	0.0130	0.979	0.0031	0.961				
5	0.0308	0.816	0.0148	0.952	0.0039	0.943				
Particle size (µm)										
315	0.0114	0.944	0.0042	0.964	0.0004	0.950				
200	0.0183	0.969	0.0073	0.990	0.0011	0.919				
122.5	0.0234	0.967	0.0101	0.993	0.0020	0.901				
60	0.0284	0.897	0.0130	0.979	0.0031	0.961				
38	0.0325	0.782	0.0159	0.937	0.0044	0.992				
Stirring speed (rpm)										
200	0.0137	0.995	0.0052	0.999	0.0006	0.906				
400	0.0163	0.961	0.0064	0.978	0.0009	0.883				
600	0.0253	0.970	0.0112	0.998	0.0024	0.927				
800	0.0284	0.897	0.0130	0.979	0.0031	0.961				
1000	0.0304	0.829	0.0145	0.958	0.0038	0.958				

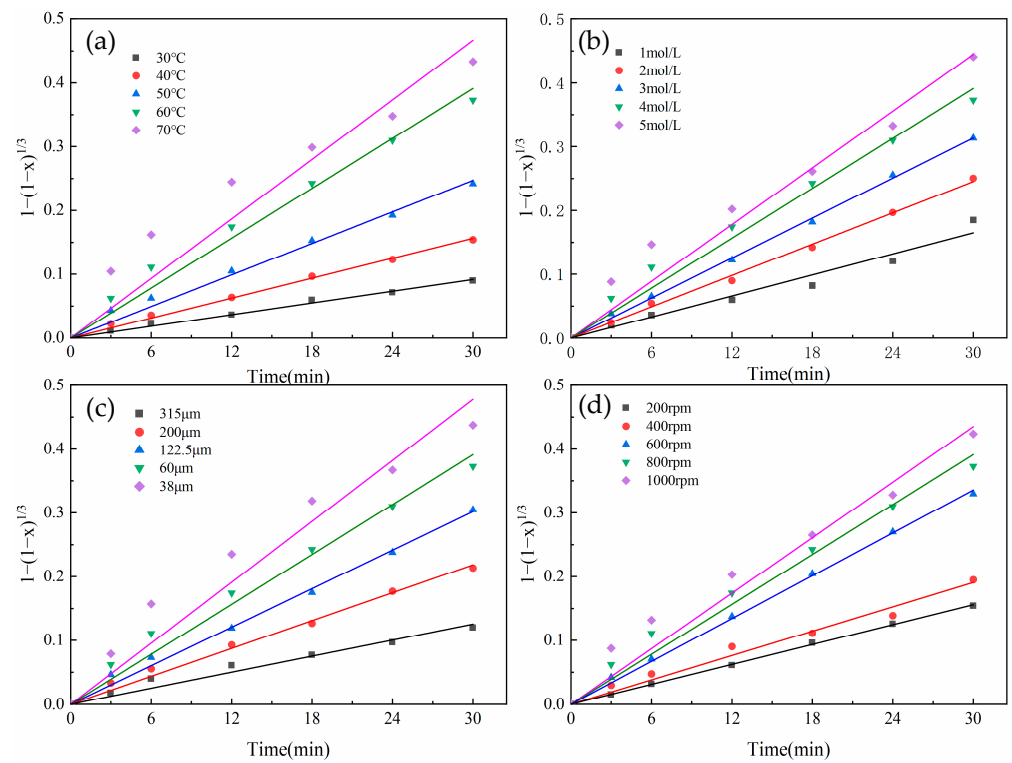


**Figure 8.** Plot of  $1 - (1 - x)^{1/3}$  versus time for various temperatures (a), solution concentrations (b), particle sizes (c), and stirring speeds (d).

It is worth mentioning that a rather large scatter of points on the kinetic curve in Figure 8 for a temperature of 70 °C ( $R^2 = 0.921$ ) indicates that the data on leaching at 70 °C do not obey the chosen model of a heterogeneous process. On the basis of previous studies, we can assume that the mechanism of the leaching process changes over time [56]. When point 0 ( $X = 0$  at  $t = 0$ ) on the kinetic curve for 60 °C and 70 °C is ignored, the selected kinetic model has a good linear relationship with temperature, as shown in Figure 9. After 3 min, the correlation coefficient  $R^2 = 0.9838$  for 60 °C and 0.9978 for 70 °C. The experimental data under these conditions can be described by the surface chemical reaction control model.

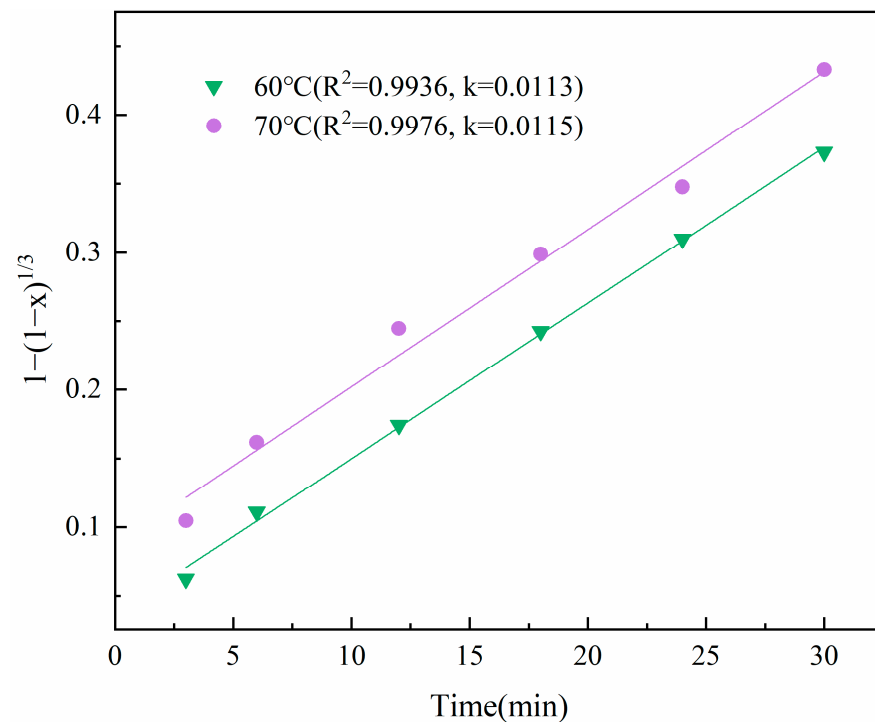


**Figure 9.** Plot of  $1 - (1 - x)^{1/3}$  versus time for 60 °C and 70 °C.

However, linearization of the data without taking into account the starting point in the approximation of the selected model will lead to a sharp change in the rate constants for temperatures of 60 °C and 70 °C. A bend will appear on the curve in the coordinates of the Arrhenius equation. Therefore, we speculate that the kinetic model will change to the internal diffusion control model when the temperature is higher than 60 °C. This means that with an increase in temperature ( $>60$  °C), the leaching rate is not only determined by the rate of chemical reaction itself, but is more influenced by the diffusion rate of products in the reaction system. The data belonging to Equation (9) in Table 5 ( $R^2 = 0.987$  for 70 °C) also support this conclusion.

### 3.7. Calculation of Activation Energy in the Leaching Process

With temperatures higher than 60 °C, the kinetic model may change. Therefore, the activation energy of the chemical reaction stage model is calculated. As seen in Figure 10, the Arrhenius graph was drawn at the study temperature using the given kinetic rate constant. And the calculated activation energy of the dissolution process was equal to 42 kJ/mol.

Thus, at a temperature not higher than 60 °C, the equation indicating the kinetics of the leaching process is obtained by

$$1 - (1 - x)^{1/3} = \left[ k_0 \cdot (C)^\alpha \cdot (r_0)^\beta \cdot (SS)^\gamma \exp(-E/RT) \right] t \quad (10)$$

where C represents the ammonium citrate concentration;  $r_0$  denotes the particle size of ore; SS is the stirring speed; E, R, and T are, respectively, the activation energy, universal gas constant, and reaction temperature;  $\alpha$ ,  $\beta$ , and  $\gamma$  are the reaction orders for relative factors; and  $k_0$  represents the pre-exponential factor.

It can be seen in Figures 11–13 that the calculated values of  $\alpha$ ,  $\beta$ , and  $\gamma$  are equal to 0.6181,  $-0.5868$ , and 0.6901, respectively. Therefore, the equation of dissolution of smithsonite in ammonium citrate solutions can be expressed as:

$$1 - (1 - x)^{1/3} = [k_0 \cdot (C)^{0.6181} \cdot (r_0)^{-0.5868} \cdot (SS)^{0.6901} \exp(-42/RT)]t \quad (11)$$

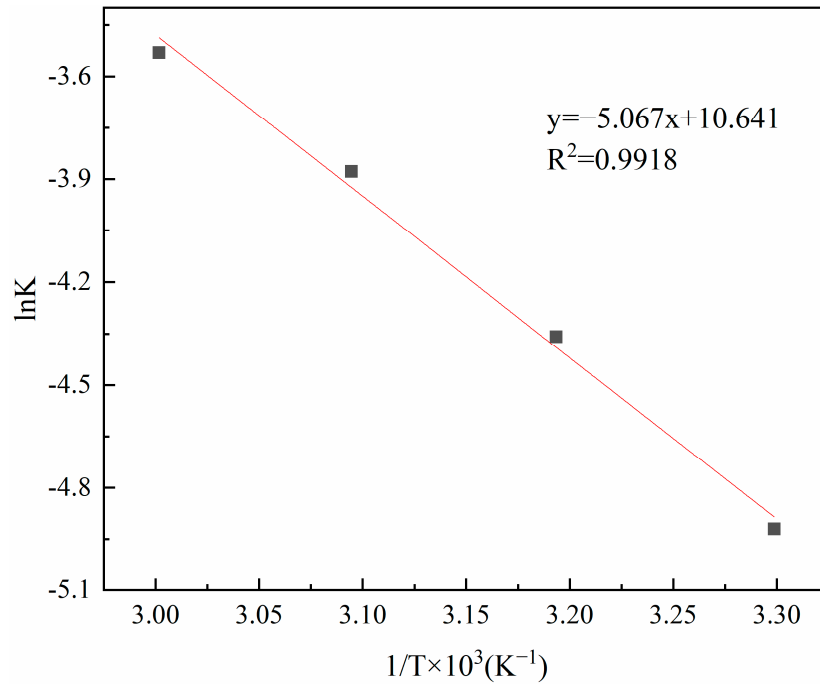


Figure 10. Arrhenius plot of smithsonite leaching—plot of ln k versus temperature.

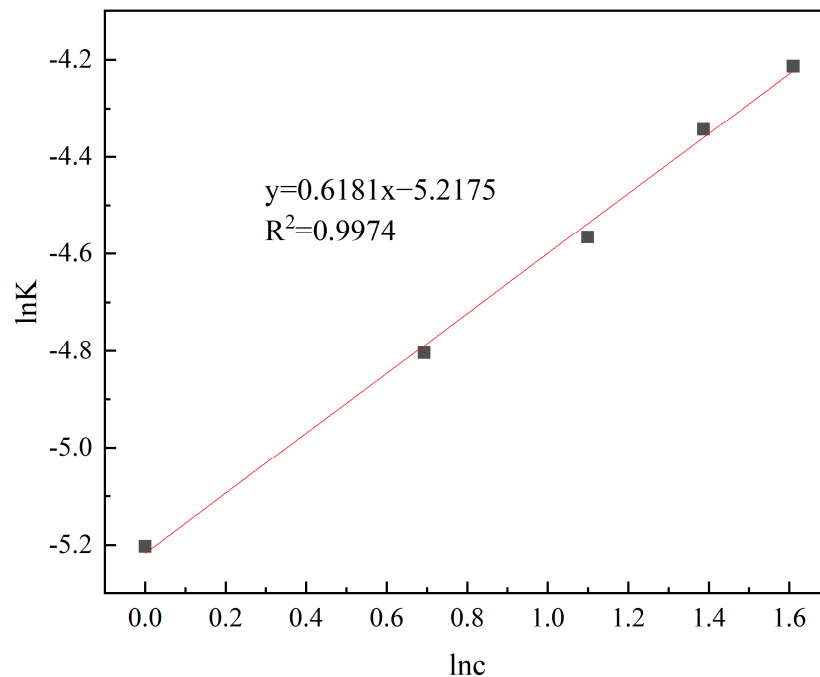
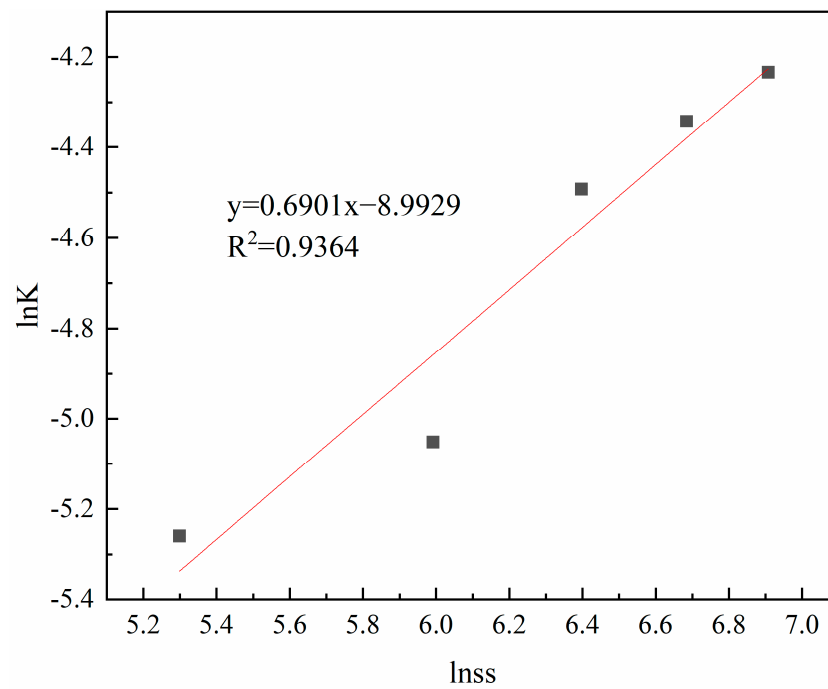
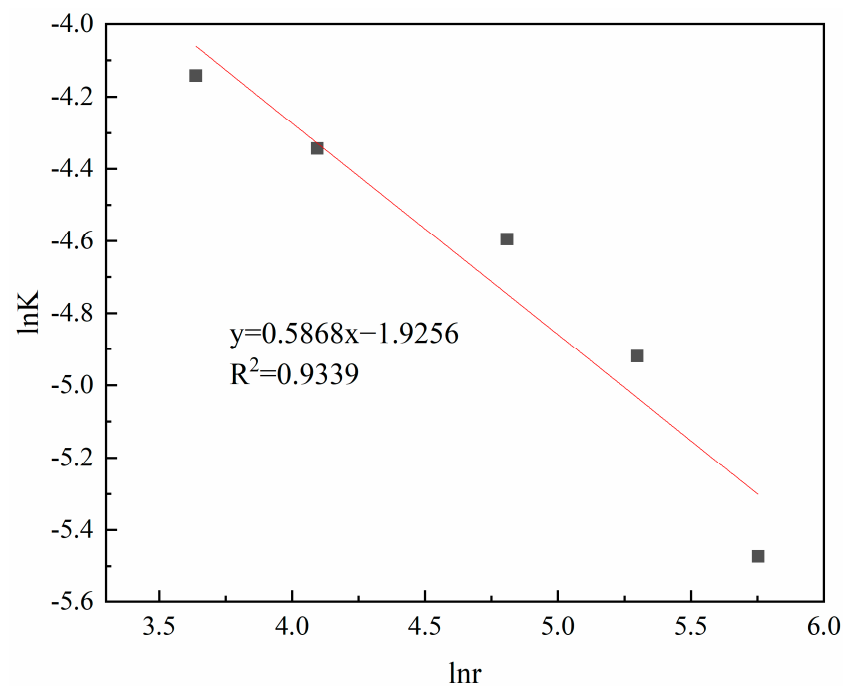


Figure 11. Plot of ln k versus ammonium citrate concentrations.



**Figure 12.** Plot of  $\ln k$  versus stirring speed.

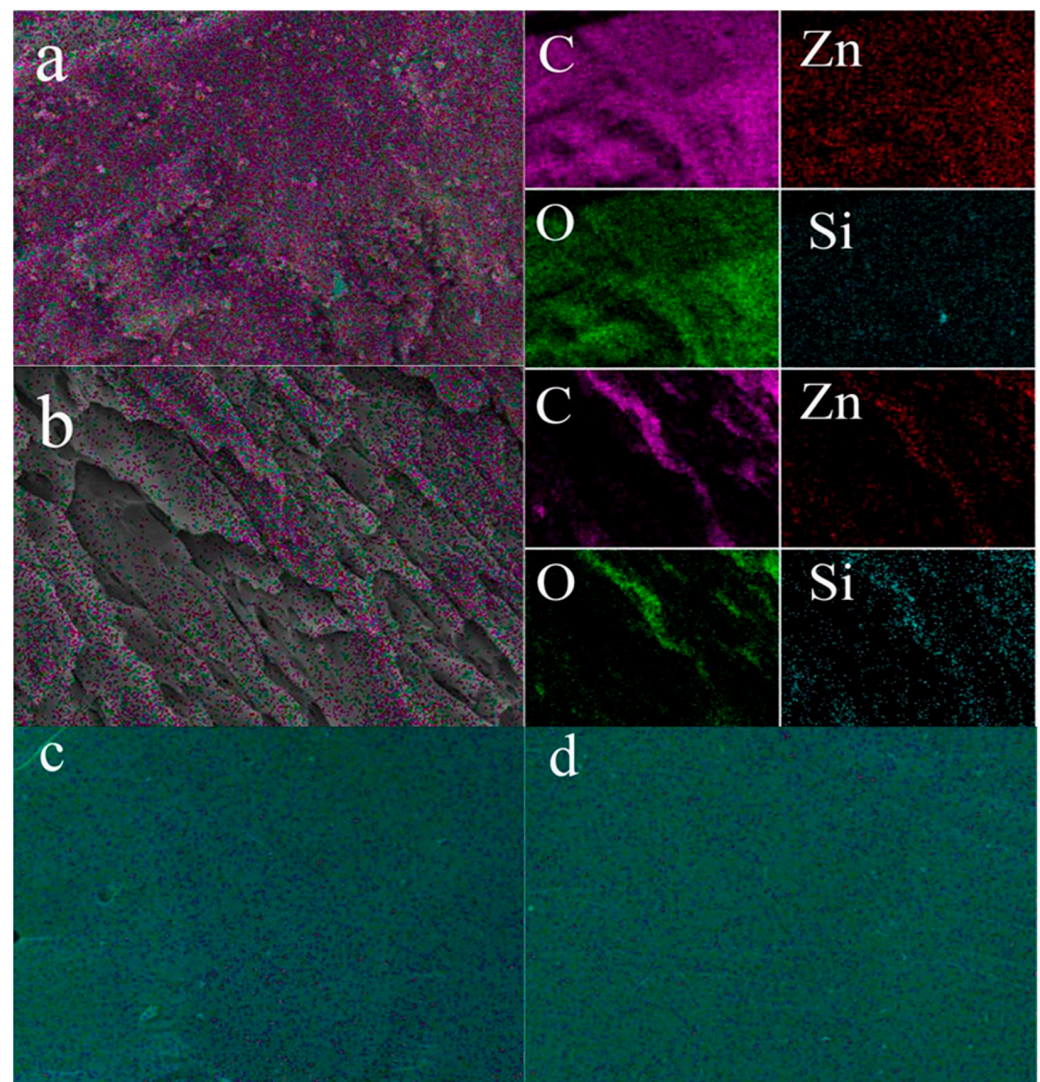


**Figure 13.** Plot of  $\ln k$  versus particle size.

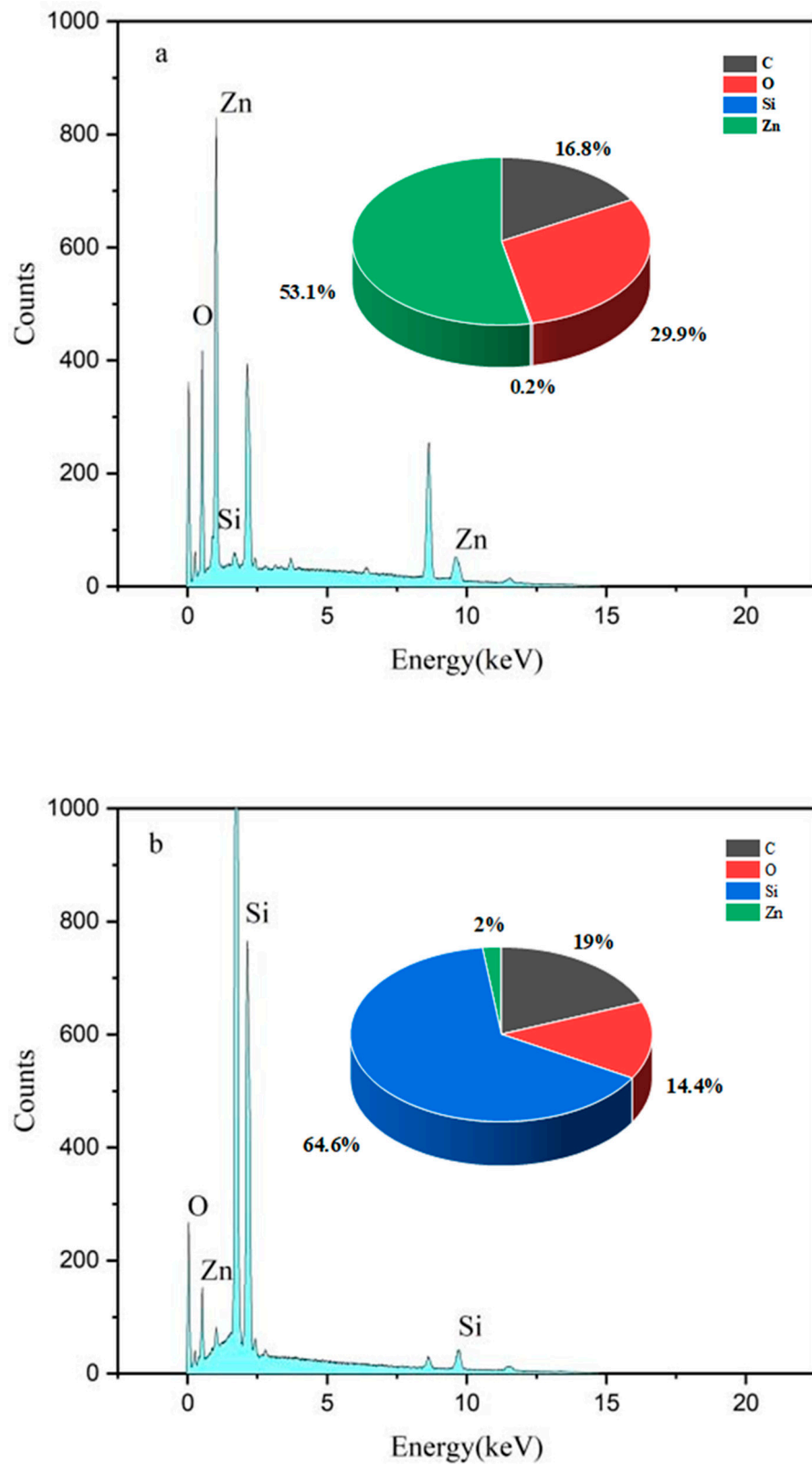
### 3.8. SEM-EDS Analysis

Figure 14 shows the surface morphology of smithsonite after leaching in ammonium citrate solution, where Figure 14a,b present the SEM morphology of smithsonite ore before leaching and that of the leaching residue, respectively. The leaching parameters were set as follows: reaction temperature of 60 °C, ammonium citrate solution concentration of 5 mol/L, particle size of 38  $\mu\text{m}$ , and stirring speed of 800 rpm. It can be seen in Figure 14a–d that the surface of the smithsonite ores is smoother than that of the leaching residue, while that of the gangue minerals remains constant during the leaching process. This is a morphological proof for explaining the selectivity of leaching in an ammonium

citrate solution. Furthermore, it can be seen that the Zn element is more distributed in ores than in leaching residue. In order to further analyze the chemical composition of the smithsonite ore and leaching residue, EDS analyses were conducted on the surfaces of two samples. Figure 15a,b present the energy spectra of the smithsonite and leaching residue, respectively. The energy spectrum depicted in Figure 15a reveals prominent peaks attributed to oxygen (O), silicon (Si), and zinc (Zn), with a notable atomic concentration of 53.1% for zinc. After the leaching process, the energy spectrum depicted in Figure 15b reveals the prominent peaks corresponding to O, Si, and Zn elements, with a noticeable decrease in the atomic concentration of Zn to 2%. Moreover, the atomic concentration of Si increased from 0.2% to 64.7% compared with the surface of non-leached smithsonite. This phenomenon demonstrates that zinc in smithsonite is fully leached in the ammonium citrate solution.



**Figure 14.** Scanning electron micrographs of smithsonite samples: (a) ore before leaching; (b) residue after leaching; (c) gangue mineral before leaching; (d) gangue mineral after leaching.



**Figure 15.** EDS spectra of raw ore and leaching residue of smithsonite ore: (a) raw ore; (b) leaching residue.

#### 4. Conclusions

This paper studies the dissolution kinetics of smithsonite in an ammonium citrate solution, and the parameters affecting the reaction. The results obtained show that an increase in the temperature, concentration of ammonium citrate solution, and stirring speed have a positive impact on the leaching rate, while an increase in the particle size has a negative impact on it. The effectiveness of ammonium citrate in the dissolution of zinc in smithsonite is then verified. Based on the experimental data, the determined optimum dissolution conditions in the tested range consist of a reaction temperature of 70 °C, an ammonium citrate solution concentration of 5 mol/L, a particle size of 38 µm, and a stirring speed of 1000 rpm. In addition, the leaching rate of zinc from smithsonite is 83.51%. Furthermore, the sufficient time determined for achieving over 80% of zinc extraction is half an hour.

Additionally, it is inferred that the shrinking core model of surface chemical reaction governs the leaching kinetics of smithsonite in an ammonium citrate solution.

It is also deduced that the leaching kinetics of smithsonite in an ammonium citrate solution is controlled by the shrinking core model of surface chemical reaction. In the temperature range of 30–70 °C, the calculated activation energy of the reaction is equal to 42 kJ/mol. The leaching rate equation can be expressed as:  $1 - (1 - x)^{1/3} = [k_0 \cdot (C)^{0.6181} \cdot (r_0)^{-0.5868} \cdot (SS)^{0.6901} \exp(-42/RT)]t$ . When the temperature is higher than 60 °C, the leaching kinetic model may change to internal diffusion control.

**Author Contributions:** H.C.: Methodology, Data curation, Investigation, Writing—original draft; D.W.: Project administration, Conceptualization, Writing—review & editing, Funding acquisition; Z.W.: Data curation, Software, Validation. All authors have read and agreed to the published version of the manuscript.

**Funding:** This research project was supported by Yunnan Fundamental Research Projects (No. 202101AT070034), Ten Thousand Talent Plans for Young Top-notch Talents of Yunnan Province (No. YNWR-QNBJ-2019-131).

**Data Availability Statement:** The data presented in this study are available on request from the corresponding author. The data are not publicly available due to privacy.

**Conflicts of Interest:** The authors declare that they have no known competing financial interest or personal relationship that could have appeared to influence the work reported in this paper.

#### References

1. Liu, W.P.; Wang, Z.X.; Wang, X.M.; Miller, J.D. Smithsonite flotation with lauryl phosphate. *Miner. Eng.* **2020**, *147*, 106155. [[CrossRef](#)]
2. Jia, K.; Lu, Y.; Liu, J.; Cheng, S.; Liu, S.; Cao, Y.; Li, G. Selective flotation separation of hemimorphite from quartz using the biosurfactant sodium N-lauroylsarcosinate as a novel collector. *Miner. Eng.* **2023**, *198*, 108073. [[CrossRef](#)]
3. Gamutan, J.; Koide, S.; Sasaki, Y.; Nagasaka, T. Selective dissolution and kinetics of leaching zinc from lime treated electric arc furnace dust by alkaline media. *J. Environ. Chem. Eng.* **2024**, *12*, 111789. [[CrossRef](#)]
4. Ye, F.; Li, M.; Su, S.; Xia, H.; Wei, C.; Li, X.; Deng, Z. Separation and recovery of zinc from blast furnace dust via coordination leaching of  $\text{Cl}^-$  and hydrolysis of  $\text{NH}_4^+$ . *Sep. Purif. Technol.* **2024**, *330*, 125361. [[CrossRef](#)]
5. Chen, C.N.; Zhang, S.; Liu, Q.J.; Chen, L.Z.; Xian, Y.J.; Wang, Y.J. Ultrasonic pretreatment for enhancing flotation separation of elemental sulfur and silver-bearing lead minerals from an oxidative pressure leaching residue of zinc sulfide. *Miner. Eng.* **2024**, *205*, 108495. [[CrossRef](#)]
6. Ge, H.; Xie, F.; Wu, S.H.; Wang, W. Biomass as a clean reductant for recovery of zinc from zinc leaching residue. *J. Clean. Prod.* **2024**, *434*, 139926. [[CrossRef](#)]
7. Feng, Q.C.; Wen, S.M.; Cao, Q.B.; Lu, C. A novel method for improving cerussite sulfidization. *Int. J. Miner. Metall. Mater.* **2016**, *23*, 609–617. [[CrossRef](#)]
8. Kursunoglu, S.; Kursunoglu, N.; Hussaini, S.; Kaya, M. Selection of an appropriate acid type for the recovery of zinc from a flotation tailing by the analytic hierarchy process. *J. Clean. Prod.* **2021**, *283*, 124659. [[CrossRef](#)]
9. Lan, Z.Y.; Lai, Z.N.; Zheng, Y.X.; Ning, J.L. Thermochemical modification for the surface of smithsonite with sulfur and its flotation response. *Miner. Eng.* **2020**, *150*, 106271. [[CrossRef](#)]
10. Yang, T.Z.; Rao, S.; Zhang, D.C.; Wen, J.F.; Liu, W.F.; Chen, L.; Zhang, X.W. Leaching of low grade zinc oxide ores in nitrilotriacetic acid solutions. *Hydrometallurgy* **2016**, *161*, 107–111. [[CrossRef](#)]

11. Abkhoshk, E.; Jorjani, E.; Al-Harashsheh, M.S.; Rashchi, F.; Naazeri, M. Review of the hydrometallurgical processing of non-sulfide zinc ores. *Hydrometallurgy* **2014**, *149*, 153–167. [[CrossRef](#)]
12. Gupta, A. *Purification, and the Energy Cost Associated with the Manufacture of Si, CdTe, and CIGS PV*; Letcher, T.M., Fthenakis, V.M., Eds.; A Comprehensive Guide to Solar Energy Systems; Academic Press: Cambridge, MA, USA, 2018; pp. 445–467.
13. Luo, Y.J.; Zhang, G.F.; Mai, Q.Y.; Liu, H.J.; Li, C.B.; Feng, H.G. Flotation separation of smithsonite from calcite using depressant sodium alginate and mixed cationic/anionic collectors. *Colloids Surf. A Physicochem. Eng. Asp.* **2020**, *586*, 124227. [[CrossRef](#)]
14. Zhao, L.; Liu, W.G.; Liu, W.B.; Zhou, S.J.; Peng, X.Y. Investigation on matching relationship between surface characters and collector properties: Achieving flotation separation of zinc oxide minerals from quartz. *Colloids Surf. A Physicochem. Eng. Asp.* **2021**, *617*, 126392. [[CrossRef](#)]
15. Liang, W.; Bai, J.; Li, Z.S.; Meng, Y.; Liu, K.X.; Li, L. Crystal growth, structure and thermal properties of anhydrous zinc carbonate (ZnCO<sub>3</sub>). *J. Alloys Compd.* **2022**, *898*, 162916. [[CrossRef](#)]
16. Jiang, T.; Meng, F.Y.; Gao, W.; Zeng, Y.; Su, H.H.; Li, Q.; Zhong, Q. Leaching behavior of zinc from crude zinc oxide dust in ammonia leaching. *J. Cent. South Univ.* **2021**, *28*, 2711–2723. [[CrossRef](#)]
17. Jha, M.K.; Kumar, V.; Singh, R.J. Review of hydrometallurgical recovery of zinc from industrial wastes. *Resour. Conserv. Recycl.* **2001**, *33*, 1–22. [[CrossRef](#)]
18. Al-Harashsheh, M.; Kingman, S.; Al-Makhadmah, L.; Hamilton, I.E. Microwave treatment of electric arc furnace dust with PVC: Dielectric characterization and pyrolysis-leaching. *J. Hazard. Mater.* **2014**, *274*, 87–97. [[CrossRef](#)]
19. Sadeghi, S.M.; Vanpeteghem, G.; Neto, I.F.F.; Soares, H.M.V.M. Selective leaching of Zn from spent alkaline batteries using environmentally friendly approaches. *Waste Manag.* **2017**, *60*, 696–705. [[CrossRef](#)] [[PubMed](#)]
20. Chen, W.; Liao, C.; Lin, K. Recovery Zinc and Manganese from Spent Battery Powder by Hydrometallurgical Route. *Energy Procedia* **2017**, *107*, 167–174. [[CrossRef](#)]
21. Havlík, T.; Souza, B.V.E.; Bernardes, A.M.; Schneider, I.A.H.; Mišková, A. Hydrometallurgical processing of carbon steel EAF dust. *J. Hazard. Mater.* **2006**, *135*, 311–318. [[CrossRef](#)]
22. Palimaka, P.; Pietrzyk, S.; Stepień, M.; Cieccko, K.; Nejman, I. Zinc Recovery from Steelmaking Dust by Hydrometallurgical Methods. *Metals* **2018**, *8*, 547. [[CrossRef](#)]
23. Hoerber, L.; Steinlechner, S. A comprehensive review of processing strategies for iron precipitation residues from zinc hydrometallurgy. *Clean. Eng. Technol.* **2021**, *4*, 100214. [[CrossRef](#)]
24. Yang, K.; Sun, C.; Qu, H.; Shuo, L.; Luo, Y.; Zhang, L.; Ma, A. Recovery of Zinc from Oxide-Sulphide Zinc Ore Through Oxidation and Chelation. In *Materials Engineering—From Ideas to Practice: An EPD Symposium in Honor of Jiann-Yang Hwang*; Springer International Publishing: Berlin/Heidelberg, Germany, 2021; pp. 161–169.
25. Kuma, C.; Obut, A. Effect of heating on structure and leaching characteristics of a zinc carbonate ore. *Physicochem. Probl. Miner. Process* **2021**, *57*, 23–32. [[CrossRef](#)]
26. Soltani, F.; Darabi, H.; Aram, R.; Ghadiri, M. Leaching and solvent extraction purification of zinc from Mehdiabad complex oxide ore. *Sci. Rep.* **2021**, *11*, 1566. [[CrossRef](#)] [[PubMed](#)]
27. Fabiano, M.F.S.; Pablo, S.P.; Rodrigo, P. The kinetics of zinc silicate leaching in sodium hydroxide. *Hydrometallurgy* **2010**, *102*, 43–49.
28. Chen, B.; Shen, X.Y.; Gu, H.M. Extracting reaction mechanism analysis of Zn and Si from zinc oxide ore by NaOH roasting method. *J. Cent. South Univ.* **2017**, *24*, 2266–2274. [[CrossRef](#)]
29. Shen, X.Y.; Shao, H.M.; Gu, H.M. Reaction mechanism analysis of roasting Zn<sub>2</sub>SiO<sub>4</sub> using NaOH. *Trans. Nonferrous Met. Soc. China* **2018**, *28*, 1878–1886. [[CrossRef](#)]
30. Chen, A.L.; Li, C.M.; Qan, Z. Hemimorphite ores: A review of processing technologies for zinc extraction. *JOM* **2016**, *68*, 2688–2697. [[CrossRef](#)]
31. Rao, S.; Zhang, D.C.; Yang, T.Z. Selective extraction of zinc from refractory hemimorphite using iminodiacetic acid as a complexing agent. *JOM* **2017**, *69*, 1909–1913. [[CrossRef](#)]
32. Rao, S.; Yang, T.Z.; Zhang, D.C. Leaching of low grade zinc oxide ores in NH<sub>4</sub>Cl–NH<sub>3</sub> solutions with nitrilotriacetic acid as complexing agents. *JOM* **2015**, *158*, 101–106. [[CrossRef](#)]
33. Wang, K.; Zhang, Q.W.; He, X.M.; Hu, H.M.; Liu, Y.C. Efficient separation of smithsonite and cerussite via mechanical ball milling-triggered selective leaching in the aqueous solution containing Pb chloride or Pb nitrate. *Hydrometallurgy* **2021**, *202*, 105589. [[CrossRef](#)]
34. Zhang, Y.D.; Hua, Y.X.; Gao, X.B.; Xu, C.Y.; Li, J.; Li, Y.; Zhang, Q.B.; Xiong, L.; Su, Z.L.; Wang, M.M.; et al. Recovery of zinc from a low-grade zinc oxide ore with high silicon by sulfuric acid curing and water leaching. *Hydrometallurgy* **2016**, *166*, 16–21. [[CrossRef](#)]
35. Wang, K.; Zhang, Q.W.; He, X.M.; Hu, H.M.; Liu, Y.C. Mechanochemical leaching of Zn from low-grade smithsonite using Fe<sub>2</sub>(SO<sub>4</sub>)<sub>3</sub> solution. *Hydrometallurgy* **2020**, *198*, 105497. [[CrossRef](#)]
36. Xu, H.S.; Wei, C.; Li, C.X.; Fan, G.; Deng, Z.G.; Zhou, X.J.; Qiu, S. Leaching of a complex sulfidic, silicate-containing zinc ore in sulfuric acid solution under oxygen pressure. *Sep. Purif. Technol.* **2012**, *85*, 206–212. [[CrossRef](#)]
37. Dhawan, N.; Safarzadeh, M.S.; Birinci, M. Kinetics of hydrochloric acid leaching of smithsonite. *Russ. J. Non-Ferr. Met.* **2011**, *52*, 209–216. [[CrossRef](#)]

38. Feng, Q.; Wen, S.; Zhao, W.; Bai, X. Dissolution regularities of smithsonite in methane sulfonic acid. *Russ. J. Non-Ferr. Met.* **2015**, *56*, 365–371. [[CrossRef](#)]
39. Zhang, Q.; Wen, S.M.; Wu, D.D.; Feng, Q.C.; Li, S. Dissolution kinetics of hemimorphite in trichloroacetic acid solutions. *J. Mater. Res. Technol.* **2019**, *8*, 1645–1652. [[CrossRef](#)]
40. Irannajad, M.; Meshkini, M.; Azadmehr, A.R. Leaching of zinc from low grade oxide ore using organic acid. *Physicochem. Probl. Miner. Process.* **2013**, *49*, 547–555.
41. Hussaini, S.; Kursunoglu, S.; Top, S.; Ichlas, Z.T. Muammer Kaya Testing of 17–different leaching agents for the recovery of zinc from a carbonate–type Pb–Zn ore flotation tailing. *Miner. Eng.* **2021**, *168*, 106935. [[CrossRef](#)]
42. Li, S.W.; Ma, A.Y.; Yang, K. Alkaline leaching of zinc from low-grade oxide zinc ore using ammonium citrate as complexing agent. *Green Process. Synth.* **2015**, *4*, 219–223. [[CrossRef](#)]
43. Zhang, L.J.; Wang, Y.; Liu, Y.L.; Lv, S.C.; Wang, R.; Hu, X.K.; Liu, Y.C.; Dong, Z.J.; Lin, K.; Liu, L. Chloride removal from sewage using bismuth trioxide: Characterization and optimization by response surface methodology (RSM). *J. Environ. Chem. Eng.* **2023**, *11*, 110868. [[CrossRef](#)]
44. Qin, J.C.; Ning, S.Y.; Zeng, J.S.; He, Z.Y.; Hu, F.T.; Li, Y.M.; Fujita, T.; Wei, Y.Z. Leaching behavior and process optimization of tin recovery from waste liquid crystal display under mechanical activation. *J. Clean. Prod.* **2023**, *399*, 136640. [[CrossRef](#)]
45. Qin, J.C.; Fujita, T.; Xu, J.N.; Wei, Y.Z.; Dodbibba, G.; Zhou, Y.L.; Li, Z.Y. Leaching behavior of indium from waste liquid crystal display: Further study on the coupling effect of multi-factors for optimum leaching process. *J. Environ. Chem. Eng.* **2022**, *10*, 107930. [[CrossRef](#)]
46. Wang, K.; Li, J.; McDonald, R.G.; Browner, R.E. The effect of iron precipitation upon nickel losses from synthetic atmospheric nickel laterite leach solutions: Statistical analysis and modelling. *Hydrometallurgy* **2011**, *109*, 140–152. [[CrossRef](#)]
47. Zhao, Q.; Liu, C.J.; Li, B.K.; Zevenhoven, R.; Saxén, H.; Jiang, M.F. Recovery of chromium from residue of sulfuric acid leaching of chromite. *Process Saf. Environ. Prot.* **2011**, *13*, 78–87. [[CrossRef](#)]
48. Peng, H.; Wang, F.; Li, G.; Guo, J.; Li, B. Highly Efficient Recovery of Vanadium and Chromium: Optimized by Response Surface Methodology. *ACS Omega* **2019**, *4*, 904–910. [[CrossRef](#)] [[PubMed](#)]
49. Tian, J.J.; Wu, D.D.; Li, S.Y.; Ma, W.H.; Wang, R.Z. Effect of process variables on leaching behavior and kinetics of silver element from waste photovoltaic modules. *Sep. Purif. Technol.* **2024**, *335*, 126062. [[CrossRef](#)]
50. Crundwell, F.K. Progress in the mathematical modelling of leaching reactors. *Hydrometallurgy* **1995**, *39*, 321–335. [[CrossRef](#)]
51. Hao, J.; Wang, X.; Wang, Y.; Wu, Y.; Guo, F. Optimizing the Leaching Parameters and Studying the Kinetics of Copper Recovery from Waste Printed Circuit Boards. *ACS Omega* **2022**, *7*, 3689–3699. [[CrossRef](#)]
52. Peng, H.; Shang, Q.; Chen, R.; Leng, Y.; Guo, J.; Liu, Z.; Tao, C. Oxidative Leaching Kinetics of Vanadium from the Vanadium-Chromium-Reducing Residue with  $K_2Cr_2O_7$ . *ACS Omega* **2020**, *5*, 8777–8783. [[CrossRef](#)]
53. Zhang, Y.J.; Sun, J.M.; Lü, G.Z.; Zhang, T.A.; Gong, Y.B. Kinetics of alumina extraction from coal gangue by hydrochloric acid leaching. *Trans. Nonferrous Met. Soc. China* **2023**, *33*, 1932–1942. [[CrossRef](#)]
54. Zoraga, M.; Ilhan, S.; Kalpakli, A.O. Leaching kinetics of electric arc furnace dust in nitric acid solutions. *Int. J. Chem. Kinet.* **2020**, *52*, 933–942. [[CrossRef](#)]
55. Li, S.J.; Zhu, J.X. Leaching kinetics of fluorine during the aluminum removal from spent Li-ion battery cathode materials. *J. Environ. Sci.* **2024**, *138*, 312–325. [[CrossRef](#)] [[PubMed](#)]
56. Dubenko, A.V.; Nikolenko, M.V.; Kostyniuk, A.; Likozar, B. Sulfuric acid leaching of altered ilmenite using thermal, mechanical and chemical activation. *Minerals* **2020**, *10*, 538. [[CrossRef](#)]

**Disclaimer/Publisher’s Note:** The statements, opinions and data contained in all publications are solely those of the individual author(s) and contributor(s) and not of MDPI and/or the editor(s). MDPI and/or the editor(s) disclaim responsibility for any injury to people or property resulting from any ideas, methods, instructions or products referred to in the content.